Au-spotted Zinc oxide nano-hexagonrods structure for plasmon-photoluminescence sensor

Akhilesh Kumar Gupta[1], Chih-Hsien Hsu[1], Ching-Hsiang Chen[2], Agnes Purwidyantri[3,4], Briliant Adhi Prabowo[1,5], Ya-Chung Tian[6], Chao-Sung Lai[1, 3, 6,7,*]

*Corresponding author: cslai@mail.cgu.edu.tw

[1]Department of Electronic Engineering, Chang Gung University, Taoyuan, Taiwan

[2]Sustainable Energy Development Center, National Taiwan University of Science & Tech., Taipei, Taiwan

[3]Biosensor Group, Chang Gung University, Taoyuan, Taiwan

[4]Research Unit for Clean Technology, Indonesian Institute of Sciences, Bandung, Indonesia

[5]Research Center for Electronics and Telecommunications, Indonesian Institute of Sciences, Bandung, Indonesia

[6]Department of Nephrology, Chang Gung Memorial Hospital, Taoyuan, Taiwan

[7]Department of Materials Engineering, Ming-Chi University of Technology, New Taipei City, Taiwan

*Corresponding author:
Prof. Chao-Sung Lai
College of Engineering, Chang Gung University
259 Wen-Hwa 1st Rd, Guishan, Taoyuan 33302, Taiwanthe
Email: cslai@mail.cgu.edu.tw
Tel: +886-3-2118800 ext. 5607
Fax:+886-3-2118700

Highlights:

- Hydrothermal synthesis of defectless Zinc Oxide nano-hexagonrods (ZnO-NH).
- Characterization of the effect of seeding temperature on ZnO-NH morphology.
- The compatibility of Au-spotted ZnO-NH surface for the plasmonic sensor.
- ZnO-NH defect correlation to photoluminescence.
- Defectless ZnO-NH effectiveness for R6G fluorescence enhancement.

Abstract:

This study presents the defectless zinc oxide nano-hexagonrods (ZnO-NH) structure decorated by gold nanoparticles (AuNPs) and its enhancement due to the tunable plasmonic field for photoluminescence sensor. The ZnO-NHs were grown on ITO glass substrate via a low cost hydrothermal method followed by annealing at different seeding temperatures, respectively. A correlation has been established between annealing temperature and the defect level concerning the diameter and density of ZnO-NH verified by Raman and FE-SEM images analysis. A further coating of the gold layer over ZnO-NH via thermal evaporator exhibits the plasmonic field enhancement in visible range which revives after short rapid annealling treatment. The enhancement is due to the large surface area of the sensing area on the haxagonrods shape and a robust plasmonic coupling between metal and ZnO which efficiently detects fluorescence signal of Rhodamine 6G (R6G) molecules. A drastic change of tunable enhanced signal was resulted byAuNPs size and morphology. and elucidated by suitable energy diagram observed from quenching to highly enhanced signal using photoluminescence spectrum and its related linearity plot. Carried out in three different thicknesses of AuNPs spotting on ZnO-NH, 3; 5 and 7 nm, it was observed that 3 nm AuNPs resulted six times higher enhancement of output signal at seeding temperature of 500°,than the 5 and 7 nm gold spotted ZnO-NH at same experimental conditions. By the proposed structure, a significant photoluminescence and plasmonics enhancement, the ease of tunability, and higher uniformity was achieved by the localized surface plasmon resonance (LSPR) from the AuNPs-decorated ZnO-NH and annealing process. Overall, the AuNPs- ZnO-NH hybrid offers a low-cost and simple fabrication potentially applied in a high-sensitive smart surface plasmonic optical sensor applications and can be a representative of new generations of photodiodes, solar cells, and metamaterials.

Keywords: Au spots, ZnO-NH (Zinc Oxide Nanohexagonrods), LSPR, annealing, photoluminescence, sensor.

1. **Introduction:**

Over the last decades, the development of plasmonic integrated devices has attracted interest for manipulating light in the nanoscale region[1–4]. Moreover, highly enhanced surface plasmons (SPs) facilitated emissions have been fascinating as seen in a wide range of general research interests in developing the band emission of ZnOmodeled metal-semiconductor nano plasmonic-based nanostructure and its related application for chemical and biology species [5,6]. Among them, metal-semiconductor study in localized surface plasmon resonance (SPR) based on gold nanoparticles (NPs) has been greatly enticing due to the rapid development of plasmonics, stability, non-toxicity, and biocompatibility of the material in the sensor surface[7–9].

On the other hand, the study of the wide- and direct-bandgap material plays an important role in the development of photonic sensor and its applications[10]. For example, the application of zinc oxide (ZnO) with its wide direct bandgap (3.7ev), large exciton binding energy (60 meV) and excellent thermal stability. Pertaining to the wide band gap of ZnO which prominently limits the light reacting range and strongly absorbs the ultraviolet range of light, most of the established works showed the trends to expand visible light response of ZnO for real-world applicationsZnO likely absorbs excitation light which further induces the creation of electron-hole pair together with charge separation. Therefore, the structuring of ZnO nanosurface is one of excellent methods to enhance both surface area to volume ratio and the photonic activity [11]. Nevertheless, common ZnO material suffers from defects as a result of impurities on its surfacewhich consequently narrows down the band emission. From this point of view, the minimization of the defects is crucialto obtain the ZnO optimum emission properties..

Numbers of latest studies have revealed that some essential properties of metal oxide semiconductors are thoroughly associated with intrinsic defects and extrinsic impurities[12,13]. However, oxygen vacancy is one of the greatest prevalent defects which can be presented into wide bandgap semiconductors to proficiently expand optical absorption range and enhance the activity of surface concerning optical sensor applications[12,13]. Wang et al. reported that oxygen vacancy could simply be formed during ZnO synthesis and the number of oxygen vacancy could be controlled by changing the annealing procedures at higher temperature [14]. This phenomena can be attributed to the decrease of the oxygen vacancies from the surface with the improvement of ZnO structure as well as strong enhancement performance of the LSPR-based biosensor [15].

LSPR is an electromagnetic oscillation created in the vicinity of noble metal nanostructures, and it is a collective oscillation model of the free conduction band electrons at the interface of noble metal NPs (Au, Ag and Cu) and semiconductor [16]. In this work, we aim to generate the LSPR field through the AuNPs decoration over ZnO-NH. This method successfully improves the plasmonic model for a high advancement strategy towards optoelectronics application. In this regard, a comprehensive investigations have presented that the composition of metal-semiconductor model correlated to the size and shape of noble metal NPs is pivotal in defining the photocatalytic efficiency of the nanohybrids materials as well as surface plasmon sensor [17].

The hybrid of semiconductors materials and metallic NPs typically provides an easy route of preparation and practical applications. Nanostructuring with different size, thickness and morphological structure of nanoparticles on a substrate emphasizes the idea towards downscaling and miniaturization towards signal augmentation [18]. For instance, it is reported that Au-TiO2 photocatalysts enhanced with 70-nm diameter of AuNPs excellently outperformed in comparison with thinner layer of AuNPs. Larger gold NPs enables larger photocatalytic activity under visible light due to stronger plasmonic resonance [19]. Furthermore,an opposite trend of ‘‘smaller is better” has been reported by Qian and coworkers who observed an enhanced photocatalytic activity for smaller NPs of 4.4 nm as being compared to the larger size of 67 nm. It was assumed that the smaller NPs yielded greater negative shift in the Fermi level which favors more effective electron transfer and charge separation [20]. She et al., investigated the effect of NPs size on the plasmonic model as well as photo catalytic activity of gold-ZnO-NH (Au@ZnO-NH) [21]. The possible ‘‘trade-off” mechanism between efficient charge transfer for smaller NPs and stronger LSPR effect for a larger one was also presented. In addition, Moirangthem et al. proved that 5nm gold thickness with NPs size of 45nm exhibited the highest sensitivity while the sample with average NPs size 96 nm showed the lowest sensitivity with respect to refractive index value [22]. A similar trend in accordance with the higher performance of the smaller particles was also reported by Nath et al., [23]. Moreover, Zheng et al. discovered the potency ofAuNPs with the size of 40 nm to retain the highest coupling effect than other NPs size when the separation of AuNPs and SPR sensing film was fixed at 5 nm. The latter work reported that the enhanced SPR sensing signals dropped with the increasing particle size, and defined the effectiveness of AuNPs with the size of 40 nm in diameter in amplifying the SPR signalthan the bigger NPs size [24]. An important fact denotes the

significance of the size anddistribution of NPs for the absorption coefficient of the dye molecule where 3 nm and 5 nm thick NPs without annealing were reported to result stronger absorption than samples with annealing and the 10 nm and 20 nm thick Ag island films were the complete opposite of this tendency [25]. Not only thata, Kim et al. also demonstrated that the quenching efficiency was lowered with the increasing size of the gold nanoparticles and the distance between dye and nanoparticles as displayed in the fluorescence spectra [26]. The reported works mostly pointed out the suitable advance model for smaller NPs size for plasmonic-based fluorescence sensor development.

In this work, we demonstrate a simple, fast and large area (1×1 cm^2) based device fabrication firstly combining thetemperature effects over ZnO-NH morphology and advantageous features toward the development of defectless ZnO surface. To reinforce the plasmonic activity, the spotting of Au on the ZnO-NH surface was conducted via thermal evaporation to avoid chemical effects over the device.The further improvement of the engineered surface was accomplished by rapid thermal treatment to target the highly predictive nature of the optical device and its enhanced optical performance. The enhanced visible emission due to gold-NPs decorated ZnO-NH, as well as Schottky based junction model and the impact of the size of the AuNPs via short rapid thermal annealing (~60 s duration) [27–30] on photoluminescence performance were scientifically studied step by step. Three device fabrication conditions were targeted for LSPR enhancement such as: (i) Defectless ZnO-NH grown on ITO, (ii) Deposition of the gold islands on ZnO-NHwith different thickness and (iii) RTA treatment.. Overall, the proposed method paves a way to establish a new model ofa simple cost-effective and less time consuming fabrication with large sensing area potentially applied forsmart plasmonic nanosensor.

2. Materials and Methods

2.1 Materials

Zinc acetate dihydrate ($Zn(OAc)_2.2H_2O$) & Rhodamine (R6G) dye were purchased from Sigma Aldrich (St. Louis, USA). Hexamethylenetetramine (HMTA) [$(CH_2)_6N_4$] were purchased from Merck (Darmstadt, Germany). Acetone, isopropyl alcohol (IPA) and toluene were purchased from Avantor (Pennsylvania, USA). ITO on a glass substrate (thickness: 0.7 mm and sheet resistance; 7Ω/square) was purchased from Uni-Onward (Taipei, Taiwan). Au evaporation slugs were purchased from Gredmann (Taipei, Taiwan). The experimental solutions were prepared using

deionized (resistivity at 25°C = 18.2 M Ωcm) water produced by a MilliQ system by Merck (Darmstadt, Germany).

2.2 Synthesis of ZnO-NH on ITO coated glass via a hydrothermal process

ZnO-NH were grown on an indium-tin oxide (ITO)-coated glass substrate (1x1 cm^2) followed by ZnO seed layers solution based low-cost hydrothermal method. Initially, the ITO glass substrates were cleaned subsequently in soap water, ethanol, IPA and de-ionized (DI) water in an ultrasonic water bath for 30 minutes each. For seed layer preparation, ITO cleaned glass substrate was wetted with 100 µL of 5 mM zinc acetate dehydrate (99%) in ethanol, rinsed with ethanol and then dried with N_2 gun. Finally, the coating steps were repeated 5 times until a homogenous coating was obtained for all substrate. After the coating process, the coated substrate was annealed at 400°C, 450°C, and 500°C in an air environment for 30 minutes by RTA model SJ-RTA1000M-V by SJ high technology (Taipei, Taiwan), respectively, to create seed layer as well as ZnO nucleation over ITO surface for the growth of ZnO-NH. The ZnO-seeded contained substrate was immersed in a Teflon beaker containing equal molar 25 mM concentration of $Zn(OAc)_2.2H_2O$ and hexamethylenetetramine ((CH2)6N4, HMTA). The aqueous solution was placed in an oven for 90°C for 8 hours [31–33]. In this process, HMTA supplies supplementary OH^- while zinc nitrate is the source of Zn^{2+} ions. Before growth, the substrate was dipped into the above solution with the ZnO seed coated film facing down. The samples were thoroughly washed with DI water to eliminate residual salt or amino complexes and allowed to dry. The schematic diagram of an experimental process and possible plasmonic model is shown in Fig.1.

Fig. 1 is preferred in this location

2.3 AuNPs spotted-ZnO-NH

The AuNPs spottend ZnO-NH hybrid was produced by the depositing Au film with the thickness of 3 or 5 or 7 nm over the defectless ZnO-NH grown at different seeding temperature via thermal evaporation with a deposition rate of 1 A˚ /s under 10^6 mTorr pressure set-up. Aiming the surface are enhancement, an RTA treatment at 650°C with 60 seconds to create AuNPs islands over ZnO-NH was applied. Figure 1 shows the schematic illustration of fabrication steps of AuNPs spotted ZnO-NH..

Fig. 2 is preferred in this location

2.4 Characterization techniques

The defectless structures of ZnO-NH at different seeding temperature was measured by Raman analysis with 473 nm laser and the steady-state PL spectrum of different samples was recorded using He-Cd laser with 405 nm diode lasers by UniDRON Co. Ltd. (New Taipei City, Taiwan).The morphology images and elemental analysis of ZnO-NH together with AuNPs spotted ZnO-NH samples before and after annealing were characterized using a field emission scanning electron microscopy combined with energy-dispersive spectroscopy (EDS) FE-SEM, JEOL-JSM-7500F (Pleasanton, CA, USA). **2.5 R6G immobilization protocols**

In this process, a 10^{-4} M of R6G probe was allowed to attach onto the AuNPs by surface adsorption process in three split conditions : ZnO-NH grown at three different seeding temperature of 400, 450 and 500°C, respectively. In addition, a blank sample without AuNPs was treated as a reference sample. All measurements were done using photoluminescence with a laser wavelength of 405 nm to observe a fluorescence peak enhancement at 570 nm of R6G molecule.

3. Results and discussions

The Raman spectrum analysis of the ZnO-NH grown under different seeding temperatures are shown in Fig. (3) with identical spectra, except for the Raman shift at E_1 (@580 cm^{-1}). The peak is reduced with the increment of the seeding temperature.. It indicates that the oxygen vacancy can be suppressed successfully as well as the improvement of the crystalline structure[14]. From the Fig. 3, it is evidence thatsee the most prominent point seen by the high-intensity sharp and robust peak at 439 cm^{-1} is attributed to the Raman active optical phonon E2 mode of ZnO confirming the productionofZnO-NH wurtzite hexagonal structure [34]. Another peak at 332 cm^{-1} represents multiple phonon scattering processes and demonstrates good tunability and suppression at high temperature.

Fig. 3 is preferred in this location

Fig. 4 (A, B, C) shows the FE-SEM images of the ZnO-NH growth at different seeding temperature and its morphological effects based on NRs diameter and density The diameter and density of ZnO-NH changes as a consequence of seeding temperature at 400, 450 and 500 °C, respectively, is closely linked with theprecursor materials coating over ITO glass [35–40]. After a successive deposition of AuNPs on ZnO-NH, Au islands over ZnO-NH structures were created as

can be observed in Fig. 4(D, E, F). Subsequently, As presented in Fig. 4 (G, H, I), the RTA greatly impacted the morphological structures of the AuNPs spotted ZnO-NH as seen in the pattern of Au embedment achieved post-RTA treatment [22,23]. Next, the morphology optimization of AuNPs thickness of 3, 5, and 7 nm on the ZnO-NH are shown in Fig. 4 (J, K, L).

The uniform density and size character of the AuNPs on ZnO-NH is presented in Fig.5 (E, F, G).These results reveals that thewhigh density of gold nanoparticles has been well-distributed on ZnO-NH via RTA treatment..

Compared to the conventional method, such as solution process[41–43], the present fabrication process using thermal evaporation and annealing offers several advantages.. First, there is no involvement of chemical reagents during the plasmonic process; therefore, it is free from surface impurities that might influence the sensing performance. Second, the size and density of AuNPs can be controlled by alternating the Au thickness in thermal evaporation procedure where it was found out that as t the deposition thickness increased from 3 to 7 nm under 650°C for 60 seconds RTA, he AuNPs size increased accordingly ().

Fig. 4 is preferred in this location

Fig. 5 is preferred in this location

As depicted in Fig. 6 (A), with the RTA ramp temperature at 650°C for 60 seconds, the highly nucleated AuNPs were observed. Whereas, the photoluminescence characterization in Fig. 6(B) displays different structures from the various treatments. TheZnO-NH with seeding temperature of 500°C and its decoration with AuNPs shows stronger intensity as being compared to other structures. Figure 6 (C, D, E) demonstrated the color changes generated by the LSPR effects on the fabricated substrate which indicates the absorption of the fraction of energy of incident light at a particular wavelength by the substrate [44–46].

Fig. 6 is preferred in this location

Fig. 7 is preferred in this location

Figure 7 shows the visible emission characteristics of ZnO-NH grown at different seeding temperature of 400, 450 and 500°C, respectively. Moreover, the study of related PL spectra in the presence and absence of AuNPs over defectless ZnO-NH carried out in the deposition of Au with different thickness of 3, 5, 7 nm via thermal evaporator was presented. PL measurements were

performed at room temperature with an excitation wavelength of 405 nm laser. RTA is an adaptable technique to yield highly reproducible and uniform plasmonic surfaces in which the embedment of the NPs on the fundamental material might be induced[22,23,47]. After RTA, PL intensity seen in the fluorescence value at 570 nm of R6G dye and its corresponding tuned linear range with respect to seeding temperature was strongly spiked due to the increment of seeding temperature during AuNPs spotted ZnO-NH fabrication for as displayed shown in Fig. 7(A to I). As a matter of fact, according to the graph defect level centering at 670 nm, the higher seeding temperatures signified the enhancement in the photoluminescence spectra of the ZnO-NH . However, after loading of R6G dye over the plasmonic surface, the green emission fluorescence value of R6G (10^{-4} M) was detected along with the defect suppression at 670 nm owning to the AuNPs size and powerful surface plasmon oscillation triggered by the visible emission from Au-spotted ZnO-NH. Importantly to point out the impact of the AuNPs size on the visible region enhancement, as seen in PL figure, the RTA of AuNPs spotted ZnO-NH at 500 °C exhibits the most significant enhancement in visible region because of fewer defects on ZnO surface than in others low temperature treatments. The thicker AuNPs represented by 7 nm thick Au film in this experiment only performed less enhancement in comparison with thinner Au deposition. This phenomenon might be occurring as as result of inadequate embedment of partial AuNPs in ZnO-NH as well as distance separation effect between AuNPs and R6G dye. This concept is a suitable novel agreement towards sensing for R6G dye and possible enhanced linearity graph altogether with potential smart surface plasmonicssensor. From the above PL results, we concluded that 650°C for 60 seconds was the most optimum temperature for controlling AuNPs size with different thickness of gold deposition over ZnO-NH and its tunable sensing behavior pertaining to seeding temperature of ZnO-NH. The structure of AuNPs spottedZnO-NH without RTA in the visible emission suppressed to the noise level as the gold layer thickness gradually increased from 3 to 7 nm. Generally, the suppression of green emission is related to AuNPs and its interaction with the ZnO structure with AuNPs.

Theoretically, the energy level of LSPR naturally enhances a strong electron transition to the higher level energy. The defect in the ZnO material is strongly correlated to the oxygen vacancy (VO) and resulting bandgap narrowing of the fabricated structure[14]. Thus, the VO forms a state level slightly above the valence band. The ZnO material with more VO contributes to the higher state level of VO above the valence band (Fig. 8 A and B). The defect level from the VO results

in the effect of seeding temperature and RTA treatment during the fabrication process. The energy transition of AuNPs-spotted ZnO-NH with high- and less-defect in ZnO crucially influences the number of electron excitation in LSPR energy level at AuNPs. The electron transition inside ZnO transition from the conduction band (CB) to the valence band (VB) is trapped by the VO and some electrons tunneling directly to the AuNPs. Due to the bandgap narrowing, the high VO results in less energy pumping to AuNPs; consequently, the electron excitation to the LSPR energy level is smaller as being compared to the defectless ZnO structure.

Moreover, the number of electron excitation in LSPR energy state also influences the electron injection to R6G and enhance the fluorescence intensity. The more electron injection in LSPR energy state, the higher intensity fluorescence of R6G. On the contrary, the number of electron in the LSPR energy state also induce sthe quenching or enhancement of electron injection to the CB of ZnO. With the absence of R6G, the PL measurement is contributed both by the energy transition of an electron to the VO (at ~670 nm) and HOMO to LUMO (at ~570 nm), in ZnO and R6G, respectively (Fig 7 A, D, G). While the the R6G induced-fluorescence intensity (at ~570 nm) has been proven by the measurement shown in Fig. 7 (B, F, H). In the case of the photoluminescence measurement without the R6G, the only intensity is contributed to the electron transition in the ZnO material. Besides, the ZnO bandgap fully depends on the oxygen vacancy that determines the defect energy level and bandgap narrowing.

Fig. 8 is preferred in this location

Fig. 9 is preferred in this location

The intensity of luminescence measurement from AuNPs spotted ZnO-NH with R6G at 570 nm of wavelength is plotted in Fig. 9. It indicates that at high seeding temperature , the ZnO-NH produced less defect on its surface and showed more effective enhancement equal to 6 times than those produced by larger and thicker AuNPs.

Finally, for a comparative study to the LSPR based optoelectronic detection, the comparison of the previously published reports and our proposed study is listed in Table 1 showing that the proposed structure is is greatly comparable to the previous reports with a significantly enhanced intensity with much simpler and cost-effective fabrication process]

Table 1 is preferred in this location.

Conclusion

In summary, we have demonstrated a simple and low-cost solution based defectless ZnO-NH at different seeding temperature to model plasmonic tunability of the interface. The further surface modification constructued in AuNPs spotted- of gold ZnO-NH structure via thermal evaporation and followed by short RTA were synergistically effective for photoluminescence signal enhancement. Results show that AuNPs over ZnO-NH prepared by short thermal annealing of 3 nm thin gold film reached the highest intensity as being compared to other thicker structure of Au. Overall, based on its low-cost model and tunable behavior in regards with AuNPs size detection capability, we envisage the proposed structure soffers the potency for various applicationsof hybrids nanocomposite for the new generations of photodiodes, solar cells, and metamaterials.

Acknowledgment

This reserach is financially supported by the Ministry of Science and Technology, Taiwan under project number MOST 107-2218-E-182-006, and Chang Gung Memorial Hospital Research Project under grant number CMRPD2F0022 and CMRPD2G0102.

Figure List and Captions:

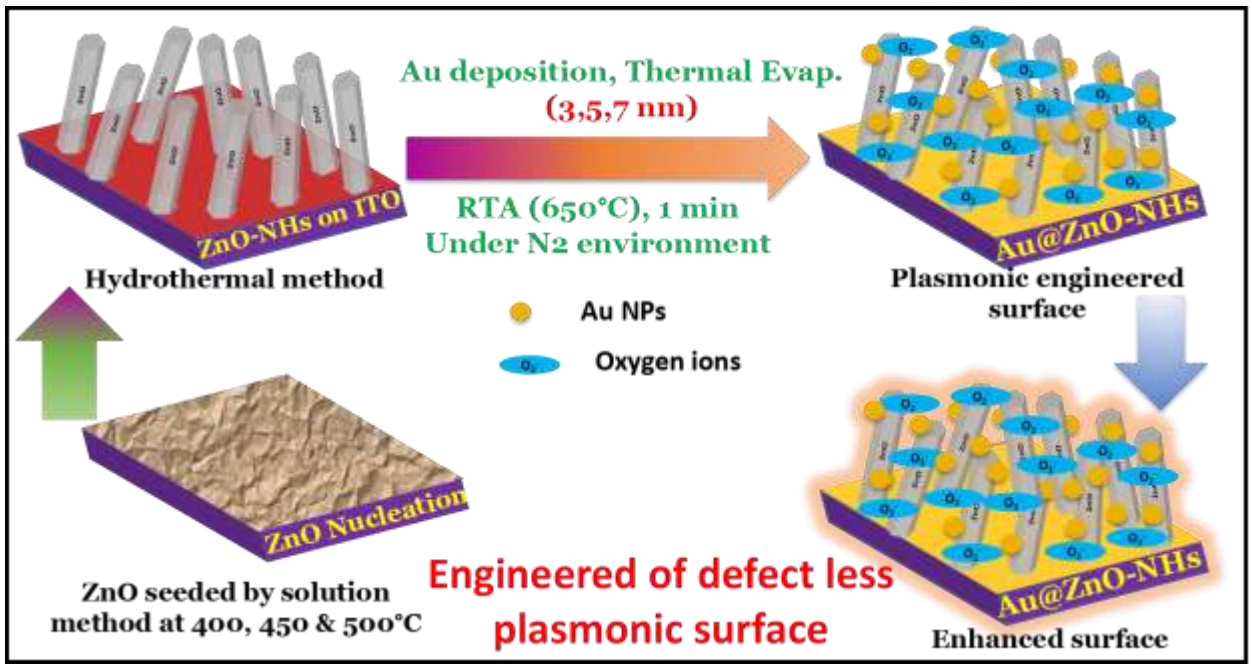

Fig. 1 Schematic illustration of ZnO-NH fabrication steps on the ITO substrate.

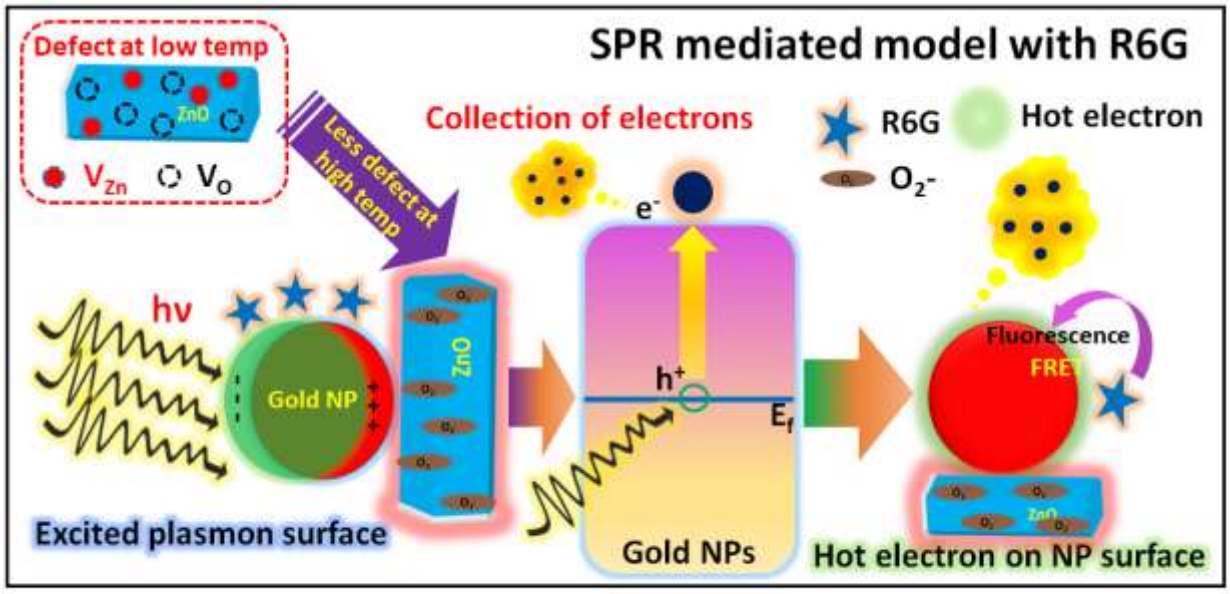

Fig. 2 The physical mechanism of the SPR mediated defectless ZnO-NH based plasmonic model for R6G detection.

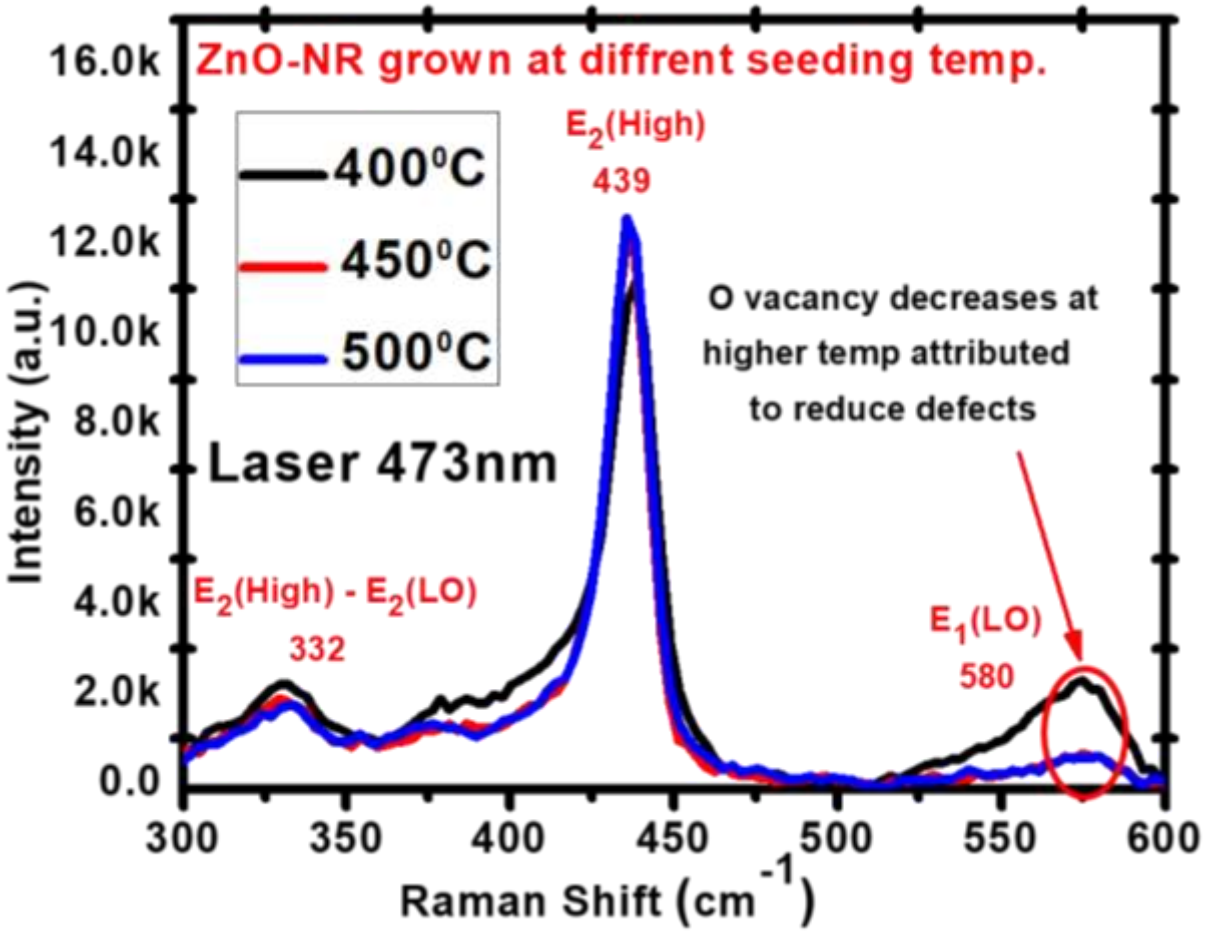

Fig. 3 Raman analysis for defect less ZnO-NH by increasing the seeding temperature.

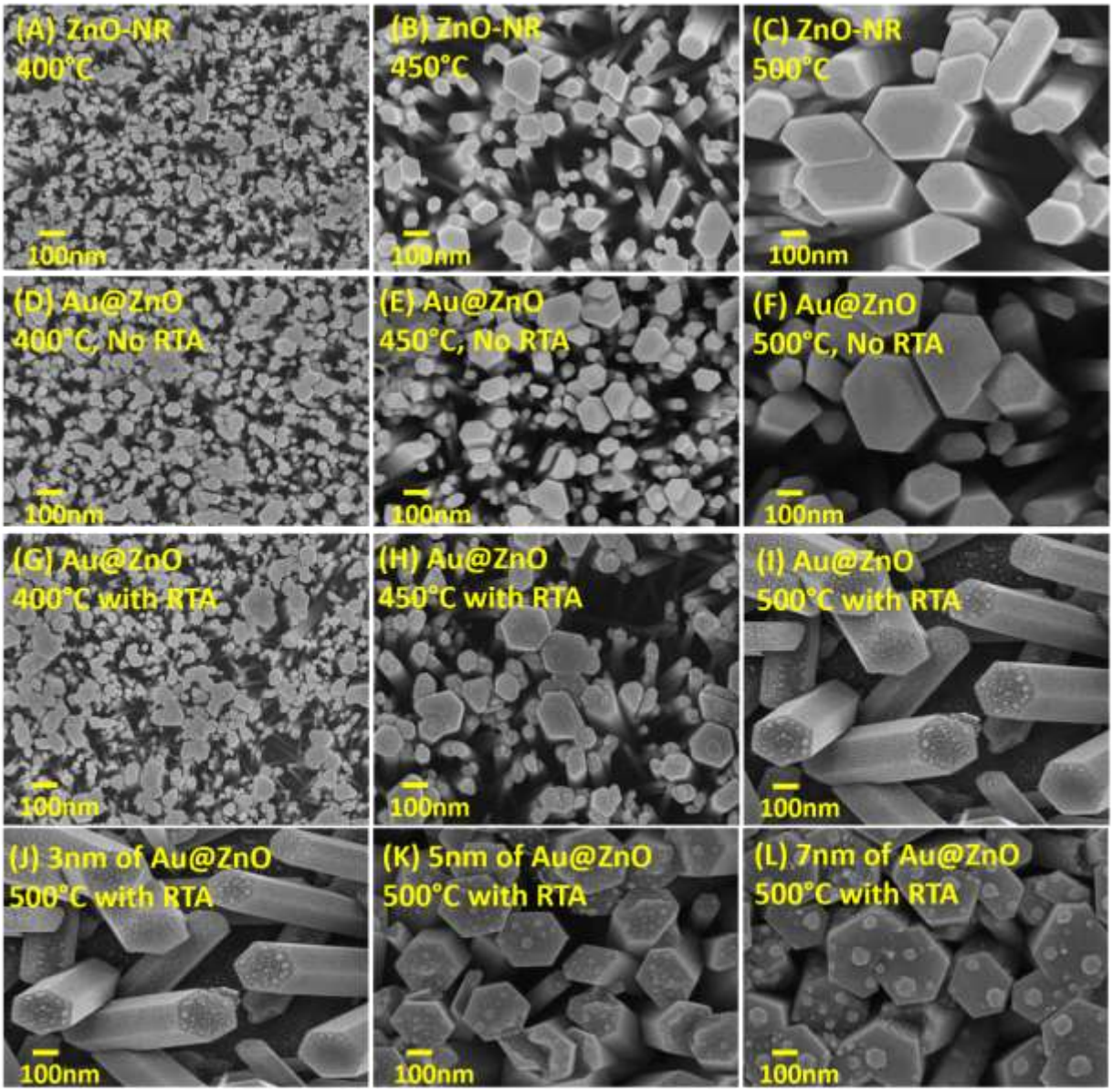

Fig. 4 FE-SEM morphology (A, B, C) ZnO-NH at different seeding temperatures. (D, E, F) The AuNPs-spotted ZnO-NH (AuNPs = 3nm) fabricated under various seeding temperatures without RTANo RTA. (G, H, I) AuNPs-spotted ZnO-NH (AuNPs = 3 nm) fabricated under various seeding temperatures with RTA -., with RTA at 650^{o}C for 30s. (J, K, L) the decoration of AuNPs with the thickness of 3, 5, and 7 nm, respectively, over ZnO-NH at seeding temperature of 500°Cpost RTA at 650^{o}C for 30s .

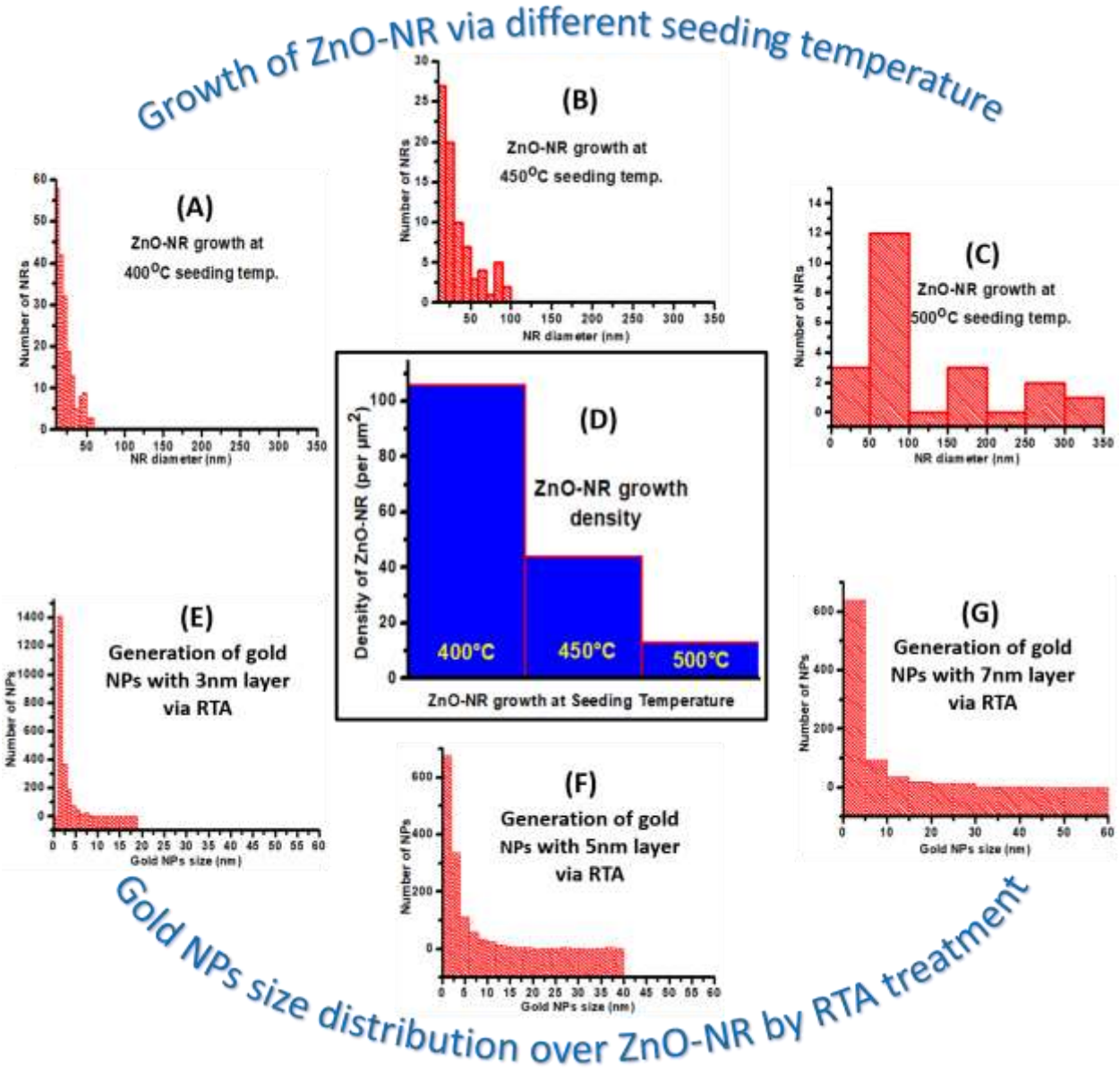

Fig. 5 Histogram plot of (A, B, C) diameter and (D) density of ZnO-NH in regards with different seeding temperatures. (E, F, G) AuNPs size tunability according to AuNPs thickness.

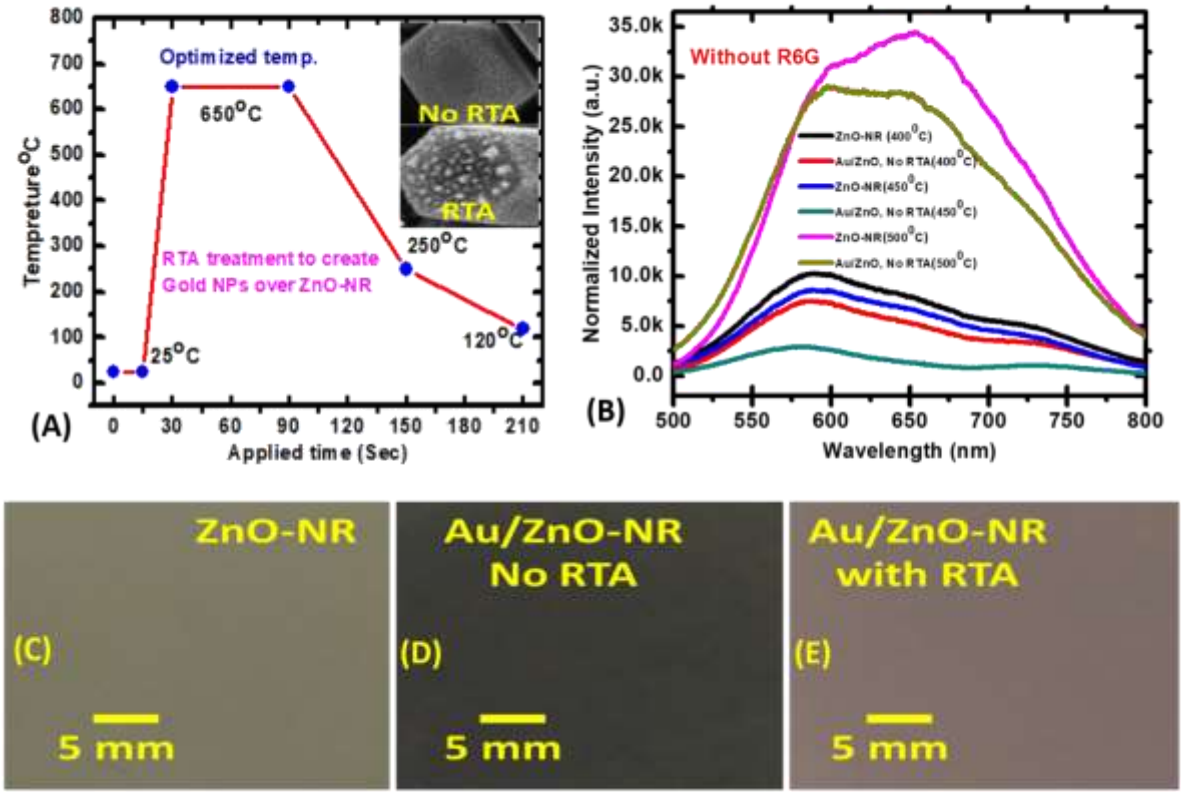

Fig. 6 (A) AuNPs creation through RTA treatment. (B) PL characteristics of different ZnO-NH substrates in the absence and presence of AuNPs, without RTA. (C, D, E) Optical images of the thin films (color changes due to the LSPR effect)

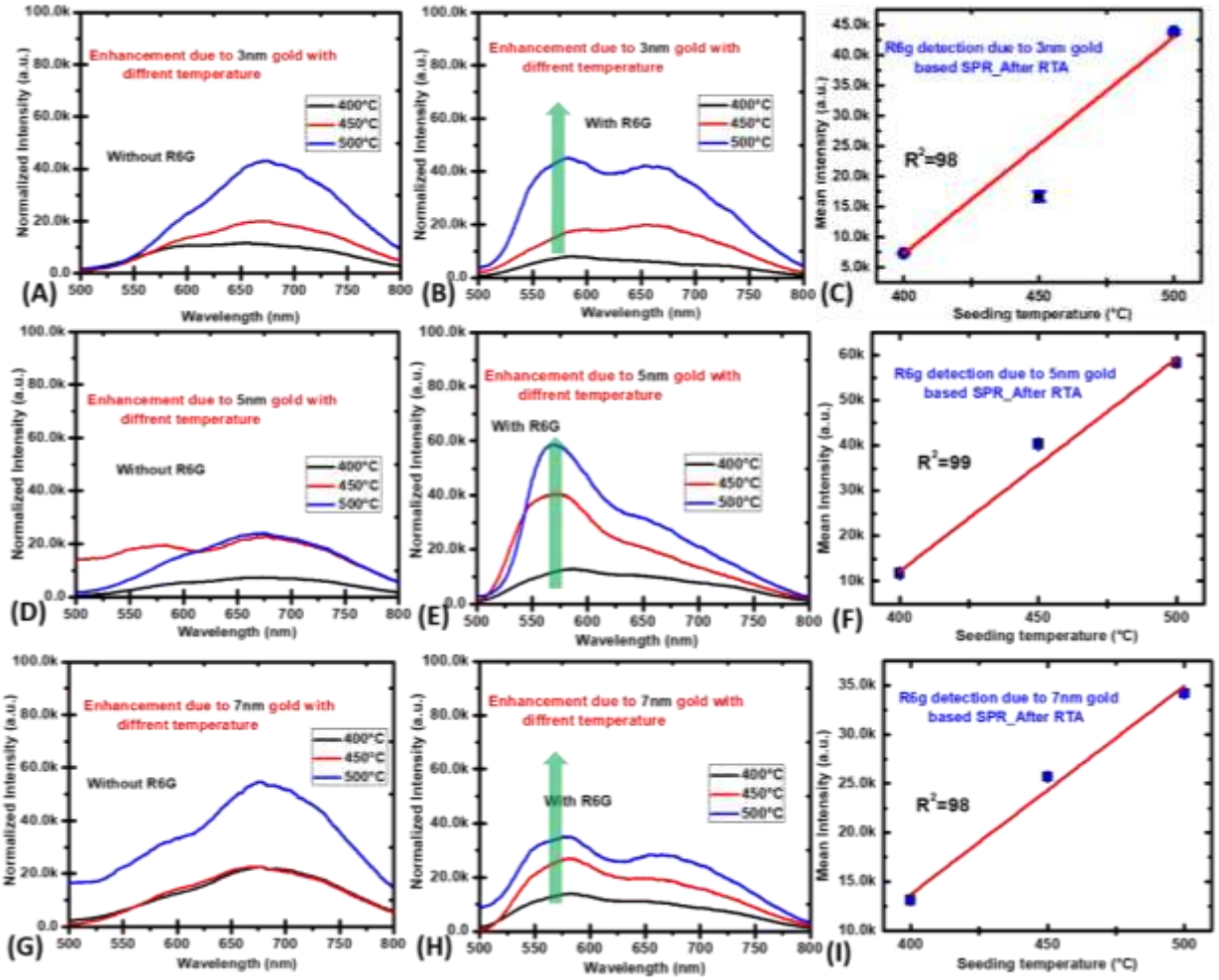

Fig. 7 Photoluminescence as well as fluorescence response studies. The fluorescence spectrum of sensing in the absence and presence of R6G of 3 nm (A, B) 5 nm (D, E), and 7 nm (G, H) Au-spotted ZnO-NH. (C, F, I) The linearity correlation of the fluorescence intensity (@570 nm of wavelength) as seeding temperature response for Au@ZnO-NH of 3 nm, 5, nm, and 7 nm, respectively and R^2 unit in percentage.

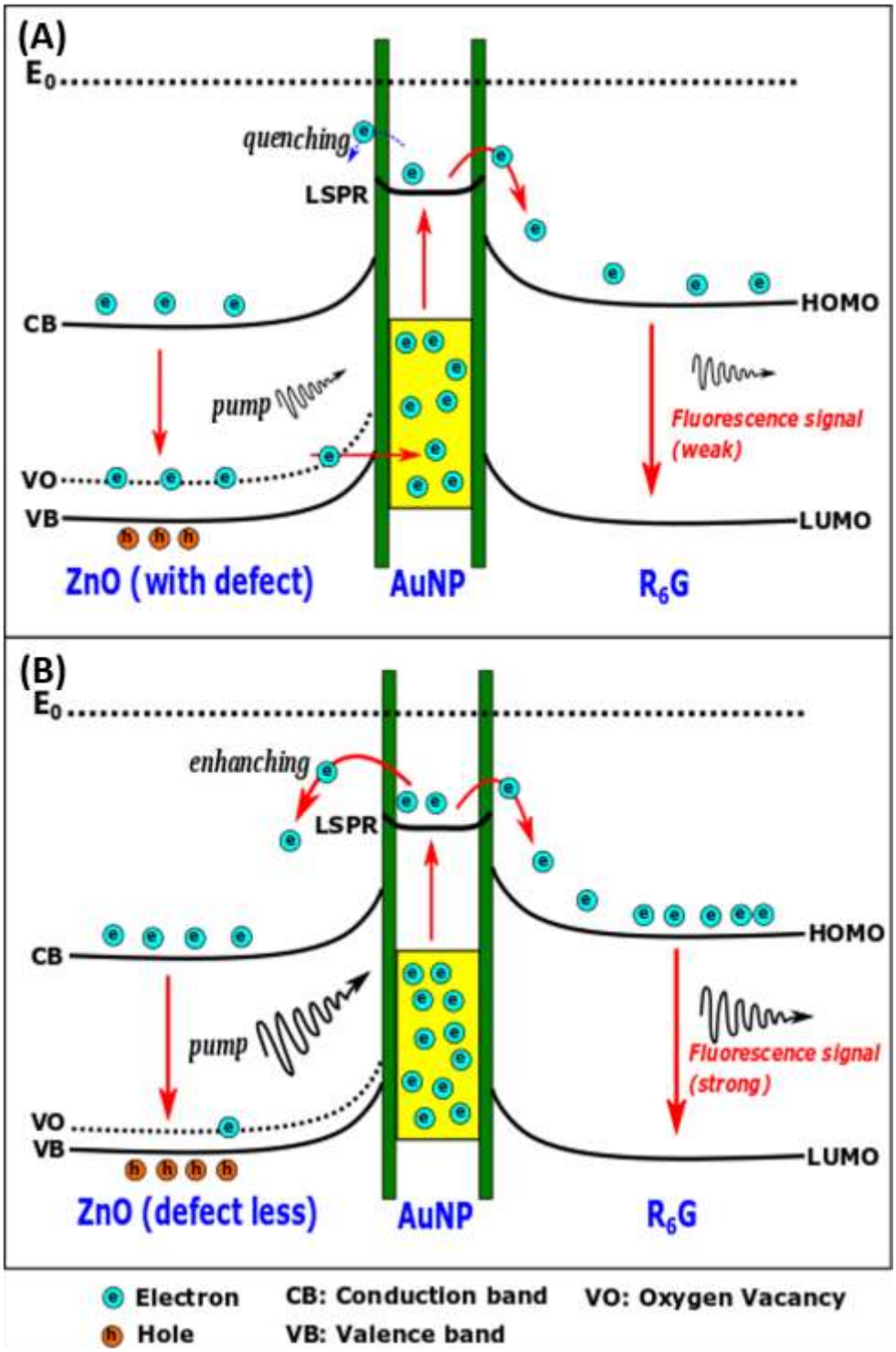

Fig. 8 Energy diagram of LSPR enhance energy transition at (A) AuNPs-spottedZnO-NH structure with a defect, and (B) defectless AuNPs-spotted ZnO-NH.

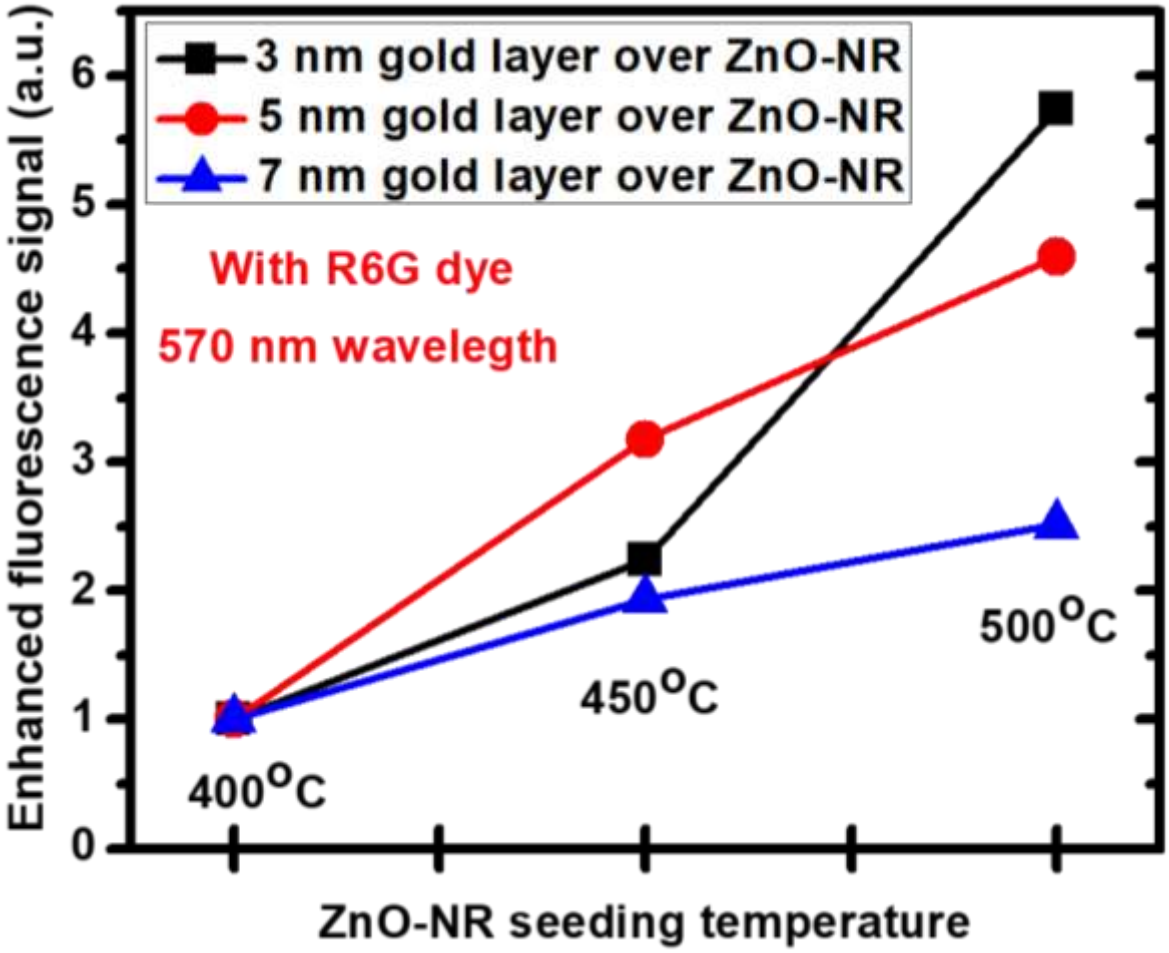

Fig. 9 Size-dependent enhanced fluorescence effects

(Please change the term ZnO-NR to ZnO-NH and gold layer to AuNPs-spotted)

Table and captions

Table 1. Comparison of the performance of previously published reports on various optoelectronic devices based on LSPR effects.

No	Types of material	Platform	Synthesis Method	Temp effect, Time	Surface morphology	Enhanced Intensity	Ref.
1	Au–ZnO	SPR	atom beam cosputtering	Anneal 600°C, 1 hour Ar atmos.	Au NPs	~ 4 times enhancement	[48]
2	Au/ZnO	SPR	Sputtering/Hydrothermal	Anneal 600°C Ar atmos.	Au NPs	~ 7 times enhancement	[45]
3	Au/ZnO (Surface plasmon)	SPR	Sputtering/ALD	n/a	Au Nanoisland	~ 2 times enhancement	[49]
4	Au-ZnO	LSPR	DC magnetron cosputtering.	Anneal 300°C, 1 hour	Au NPs	~ 2 times enhancement	[50]
5	Au/Glass	LSPR	E-beam & sputtering	RTA at 900°C, 5 min.	Au NPs	~ 7 times enhancement	[27]
6	Au/Silica	SPR	ion implanter	Anneal 950°C, 1hour Ar atmos.	Au NPs	~ 3 times enhancement	[51]
7	Au/ZnO	SPR	Wet chemical process	Anneal 600 °C for 1hr in oxygen	Au NPs	~ 7 times enhancement	[52]
8	Au/ZnO	LSPR	Sputtering/ vapor phase transport (VPT)	n/a	Au NPs	~ 2.8 times enhancement	[53]
9	Cr/ZnO	LSPR	Sputtering/ Hydrothermal	Anneal 500°	Cr NPs	~ 5 times enhancement	[54]
10	Au/ZnO-NH	LSPR	Thermal evaporator/ Hydrothermal low-cost solution based.	RTA at 650°C, 1 min. (60 seconds)	Tunable gold NPs size uniformly over ZnO-NH	~ 6 times enhancement compare than another temp.	This work

References:

[1] W. Vandezande, K.P.F. Janssen, F. Delport, R. Ameloot, D.E. De Vos, J. Lammertyn, M.B.J. Roeffaers, Parts per Million Detection of Alcohol Vapors via Metal Organic Framework Functionalized Surface Plasmon Resonance Sensors, Anal. Chem. 89 (2017) 4480–4487. doi:10.1021/acs.analchem.6b04510.

[2] J. Zhao, S. Cao, C. Liao, Y. Wang, G. Wang, X. Xu, C. Fu, G. Xu, J. Lian, Y. Wang, Surface plasmon resonance refractive sensor based on silver-coated side-polished fiber, Sensors Actuators, B Chem. 230 (2016) 206–211. doi:10.1016/j.snb.2016.02.020.

[3] B.A. Prabowo, Y.-F.F. Chang, H.-C.C. Lai, A. Alom, P. Pal, Y.-Y.Y. Lee, N.-F.F. Chiu, K. Hatanaka, L.-C.C. Su, K.-C.C. Liu, Rapid screening of Mycobacterium tuberculosis complex (MTBC) in clinical samples by a modular portable biosensor, Sensors Actuators B. Chem. 254 (2018) 742–748. doi:10.1016/j.snb.2017.07.102.

[4] B.A. Prabowo, A. Purwidyantri, K.-C. Liu, Surface Plasmon Resonance Optical Sensor: A Review on Light Source Technology, Biosensors. 8 (2018) 80. doi:https://doi.org/10.3390/bios8030080.

[5] K. Aslan, I. Gryczynski, J. Malicka, E. Matveeva, J.R. Lakowicz, C.D. Geddes, Metal-enhanced fluorescence: an emerging tool in biotechnology, Curr. Opin. Biotechnol. 16 (2005) 55–62. doi:10.1016/J.COPBIO.2005.01.001.

[6] J. Homola, Surface plasmon resonance sensors for detection of chemical and biological species, Chem. Rev. 108 (2008) 462–93. doi:10.1021/cr068107d.

[7] J.J. Homola, S.S. Yee, G.G. Gauglitz, Surface plasmon resonance sensors: review, Sens. Actuators B. 54 (1999) 3–15.

[8] J. Cao, T. Sun, K.T.V. Grattan, Gold nanorod-based localized surface plasmon resonance biosensors: A review, Sensors Actuators, B Chem. (2014). doi:10.1016/j.snb.2014.01.056.

[9] A. Zuber, M. Purdey, E. Schartner, C. Forbes, B. Van Der Hoek, D. Giles, A. Abell, T. Monro, H. Ebendorff-Heidepriem, Detection of gold nanoparticles with different sizes using absorption and fluorescence based method, Sensors Actuators, B Chem. (2016). doi:10.1016/j.snb.2015.12.044.

[10] D. Zhang, Y. Lu, J. Jiang, Q. Zhang, Y. Yao, P. Wang, B. Chen, Q. Cheng, G.L. Liu, Q. Liu, Nanoplasmonic biosensor: Coupling electrochemistry to localized surface plasmon resonance spectroscopy on nanocup arrays, Biosens. Bioelectron. (2015). doi:10.1016/j.bios.2014.08.022.

[11] Z. Yi, J. Chen, J. Luo, Y. Yi, X. Kang, X. Ye, P. Bi, X. Gao, Y. Yi, Y. Tang, Surface-Plasmon-Enhanced Band Emission and Enhanced Photocatalytic Activity of Au Nanoparticles-Decorated ZnO Nanorods, Plasmonics. 10 (2015) 1373–1380. doi:10.1007/s11468-015-9933-2.

[12] K. Jug, V.A. Tikhomirov, Influence of intrinsic defects on the properties of zinc oxide, J. Comput. Chem. 29 (2008) 2250–2254. doi:10.1002/jcc.20978.

[13] A.A. Sokol, S.A. French, S.T. Bromley, C.R.A. Catlow, H.J.J. Van Dam, P. Sherwood,

Point defects in ZnO, in: Faraday Discuss., 2007. doi:10.1039/b607406e.

[14] J. Wang, Z. Wang, B. Huang, Y. Ma, Y. Liu, X. Qin, X. Zhang, Y. Dai, Oxygen vacancy induced band-gap narrowing and enhanced visible light photocatalytic activity of ZnO, ACS Appl. Mater. Interfaces. (2012). doi:10.1021/am300835p.

[15] J. Shu, Z. Qiu, S. Lv, K. Zhang, D. Tang, Plasmonic Enhancement Coupling with Defect-Engineered TiO2–x: A Mode for Sensitive Photoelectrochemical Biosensing, Anal. Chem. 90 (2018) 2425–2429. doi:10.1021/acs.analchem.7b05296.

[16] X. Zhou, G. Liu, J. Yu, W. Fan, Surface plasmon resonance-mediated photocatalysis by noble metal-based composites under visible light, J. Mater. Chem. (2012). doi:10.1039/c2jm31902k.

[17] Y. Horiguchi, T. Kanda, K. Torigoe, H. Sakai, M. Abe, Preparation of gold/silver/titania trilayered nanorods and their photocatalytic activities, Langmuir. (2014). doi:10.1021/la404370s.

[18] A. Purwidyantri, L. Kamajaya, C.-H. Chen, J.-D. Luo, C.-C. Chiou, Y.-C. Tian, C.-Y. Lin, C.-M. Yang, C.-S. Lai, A colloidal nanopatterning and downscaling of a highly periodic au nanoporous EGFET biosensor, J. Electrochem. Soc. 165 (2018) H3170–H3177. doi:10.1149/2.0241804jes.

[19] Z.W. Seh, S. Liu, M. Low, S.Y. Zhang, Z. Liu, A. Mlayah, M.Y. Han, Janus Au-TiO2photocatalysts with strong localization of plasmonic near-fields for efficient visible-light hydrogen generation, Adv. Mater. (2012). doi:10.1002/adma.201104241.

[20] K. Qian, B.C. Sweeny, A.C. Johnston-Peck, W. Niu, J.O. Graham, J.S. Duchene, J. Qiu, Y.C. Wang, M.H. Engelhard, D. Su, E.A. Stach, W.D. Wei, Surface plasmon-driven water reduction: Gold nanoparticle size matters, J. Am. Chem. Soc. (2014). doi:10.1021/ja504097v.

[21] P. She, K. Xu, S. Zeng, Q. He, H. Sun, Z. Liu, Investigating the size effect of Au nanospheres on the photocatalytic activity of Au-modified ZnO nanorods, J. Colloid Interface Sci. 499 (2017) 76–82. doi:10.1016/J.JCIS.2017.03.089.

[22] R.S. Moirangthem, M.T. Yaseen, P.-K. Wei, J.-Y. Cheng, Y.-C. Chang, Enhanced localized plasmonic detections using partially-embedded gold nanoparticles and ellipsometric measurements, Biomed. Opt. Express. (2012). doi:10.1103/PhysRevA.37.1858.

[23] N. Nath, A. Chilkoti, Label-free biosensing by surface plasmon resonance of nanoparticles on glass: Optimization of nanoparticle size, Anal. Chem. (2004). doi:10.1021/ac049741z.

[24] S. Zeng, X. Yu, W.C. Law, Y. Zhang, R. Hu, X.Q. Dinh, H.P. Ho, K.T. Yong, Size dependence of Au NP-enhanced surface plasmon resonance based on differential phase measurement, Sensors Actuators, B Chem. (2013). doi:10.1016/j.snb.2012.09.073.

[25] K.C. Lee, S.J. Lin, C.H. Lin, C.S. Tsai, Y.J. Lu, Size effect of Ag nanoparticles on surface plasmon resonance, Surf. Coatings Technol. (2008). doi:10.1016/j.surfcoat.2008.06.080.

[26] C.K. Kim, R.R. Kalluru, J.P. Singh, A. Fortner, J. Griffin, G.K. Darbha, P.C. Ray, Gold-

nanoparticle-based miniaturized laser-induced fluorescence probe for specific DNA hybridization detection: Studies on size-dependent optical properties, Nanotechnology. (2006). doi:10.1088/0957-4484/17/13/001.

[27] H.T.-H. Lin, C.-K. Yang, C.-C. Lin, A.M.-H. Wu, L.A. Wang, N.-T. Huang, A Large-Area Nanoplasmonic Sensor Fabricated by Rapid Thermal Annealing Treatment for Label-Free and Multi-Point Immunoglobulin Sensing, Nanomaterials. 7 (2017). doi:10.3390/nano7050100.

[28] N. Bhalla, D. Lee, S. Sathish, A.Q. Shen, Dual-mode refractive index and charge sensing to investigate complex surface chemistry on nanostructures, Nanoscale. (2017). doi:10.1039/c6nr07664e.

[29] A.M. Lopatynskyi, V.K. Lytvyn, V.I. Nazarenko, L.J. Guo, B.D. Lucas, V.I. Chegel, Au nanostructure arrays for plasmonic applications: annealed island films versus nanoimprint lithography, Nanoscale Res. Lett. (2015). doi:10.1186/s11671-015-0819-1.

[30] K. Jia, J.L. Bijeon, P.M. Adam, R.E. Ionescu, Sensitive localized surface plasmon resonance multiplexing protocols, Anal. Chem. (2012). doi:10.1021/ac301825a.

[31] A. Purwidyantri, C.-H. Chen, L.-Y. Chen, C.-C. Chen, J.-D. Luo, C.-C. Chiou, Y.-C. Tian, C.-Y. Lin, C.-M. Yang, H.-C. Lai, C.-S. Lai, Speckled ZnO Nanograss Electrochemical Sensor for Staphylococcus epidermidis Detection, J. Electrochem. Soc. 164 (2017) B205–B211.

[32] S. Tiwari, M. Vinchurkar, V.R. Rao, G. Garnier, Zinc oxide nanorods functionalized paper for protein preconcentration in biodiagnostics, Sci. Rep. (2017). doi:10.1038/srep43905.

[33] L.Y. Chen, Y.T. Yin, C.H. Chen, J.W. Chiou, Influence of polyethyleneimine and ammonium on the growth of ZnO nanowires by hydrothermal method, J. Phys. Chem. C. (2011). doi:10.1021/jp2056199.

[34] Y.J. Xing, Z.H. Xi, Z.Q. Xue, X.D. Zhang, J.H. Song, R.M. Wang, J. Xu, Y. Song, S.L. Zhang, D.P. Yu, Optical properties of the ZnO nanotubes synthesized via vapor phase growth, Appl. Phys. Lett. 83 (2003) 1689–1691. doi:10.1063/1.1605808.

[35] S.Y. Liu, T. Chen, J. Wan, G.P. Ru, B.Z. Li, X.P. Qu, The effect of pre-annealing of sputtered ZnO seed layers on growth of ZnO nanorods through a hydrothermal method, Appl. Phys. A Mater. Sci. Process. (2009). doi:10.1007/s00339-008-4957-5.

[36] J.S. Huang, C.F. Lin, Influences of ZnO sol-gel thin film characteristics on ZnO nanowire arrays prepared at low temperature using all solution-based processing, J. Appl. Phys. (2008). doi:10.1063/1.2828172.

[37] M. Wang, J. Wang, W. Chen, Y. Cui, L. Wang, Effect of preheating and annealing temperatures on quality characteristics of ZnO thin film prepared by sol-gel method, Mater. Chem. Phys. (2006). doi:10.1016/j.matchemphys.2005.07.072.

[38] Q. Ahsanulhaq, J.H. Kim, Y.B. Hahn, Controlled selective growth of ZnO nanorod arrays and their field emission properties, Nanotechnology. (2007). doi:10.1088/0957-4484/18/48/485307.

[39] D. Raoufi, T. Raoufi, The effect of heat treatment on the physical properties of sol-gel derived ZnO thin films, Appl. Surf. Sci. 255 (2009) 5812–5817.

[40] U. Chaitra, D. Kekuda, K. Mohan Rao, Effect of annealing temperature on the evolution of structural, microstructural, and optical properties of spin coated ZnO thin films, Ceram. Int. 43 (2017) 7115–7122. doi:10.1016/j.ceramint.2017.02.144.

[41] F. Xu, H.F. Lv, S.Y. Wu, H.P. HO, Light-activated gas sensing activity of ZnO nanotetrapods enhanced by plasmonic resonant energy from Au nanoparticles, Sensors Actuators, B Chem. (2018). doi:10.1016/j.snb.2017.12.128.

[42] K. Liu, Y. Bi, S. Qu, F. Tan, D. Chi, S. Lu, Y. Li, Y. Kou, Z. Wang, Efficient hybrid plasmonic polymer solar cells with Ag nanoparticle decorated TiO2nanorods embedded in the active layer, Nanoscale. (2014). doi:10.1039/c4nr00030g.

[43] T. Bora, D. Zoepfl, J. Dutta, Importance of Plasmonic Heating on Visible Light Driven Photocatalysis of Gold Nanoparticle Decorated Zinc Oxide Nanorods, Sci. Rep. (2016). doi:10.1038/srep26913.

[44] T. Endo, K. Kerman, N. Nagatani, H.M. Hiepa, D.K. Kim, Y. Yonezawa, K. Nakano, E. Tamiya, Multiple label-free detection of antigen-antibody reaction using localized surface plasmon resonance-based core-shell structured nanoparticle layer nanochip, Anal. Chem. (2006). doi:10.1021/ac0608321.

[45] A. Kushwaha, M. Aslam, Defect controlled water splitting characteristics of gold nanoparticle functionalized ZnO nanowire films, RSC Adv. (2014). doi:10.1039/c4ra00782d.

[46] H. Sun, M. Yu, G. Wang, X. Sun, J. Lian, Temperature-dependent morphology evolution and surface plasmon absorption of ultrathin gold island films, J. Phys. Chem. C. (2012). doi:10.1021/jp300260h.

[47] A. Purwidyantri, I. El-Mekki, C.-S. Lai, Tunable Plasmonic SERS Hotspots on Au-Film over Nanosphere by Rapid Thermal Annealing, IEEE Trans. Nanotechnol. 16 (2017) 551–559. doi:10.1109/TNANO.2016.2647263.

[48] Y.K. Mishra, S. Mohapatra, R. Singhal, D.K. Avasthi, D.C. Agarwal, S.B. Ogale, Au-ZnO: A tunable localized surface plasmonic nanocomposite, Appl. Phys. Lett. (2008). doi:10.1063/1.2838302.

[49] R. Viter, Z. Balevicius, A. Abou Chaaya, I. Baleviciute, S. Tumenas, L. Mikoliunaite, A. Ramanavicius, Z. Gertnere, A. Zalesska, V. Vataman, V. Smyntyna, D. Erts, P. Miele, M. Bechelany, The influence of localized plasmons on the optical properties of Au/ZnO nanostructures, J. Mater. Chem. C. 3 (2015) 6815–6821. doi:10.1039/C5TC00964B.

[50] W. Chamorro, J. Ghanbaja, Y. Battie, A.E. Naciri, F. Soldera, F. Mücklich, D. Horwat, Local Structure-Driven Localized Surface Plasmon Absorption and Enhanced Photoluminescence in ZnO-Au Thin Films, J. Phys. Chem. C. 120 (2016) 29405–29413. doi:10.1021/acs.jpcc.6b09974.

[51] K.D. Devi, S. Ojha, F. Singh, Influence of thermal annealing and radiation enhanced diffusion processes on surface plasmon resonance of gold implanted dielectric matrices,

Radiat. Phys. Chem. (2018). doi:10.1016/j.radphyschem.2017.11.022.

[52] N. Gogurla, S. Bayan, P. Chakrabarty, S.K. Ray, Plasmon mediated enhancement of visible light emission of Au-ZnO nanocomposites, J. Lumin. (2018). doi:10.1016/j.jlumin.2017.09.044.

[53] F.F. Qin, C.X. Xu, Q.X. Zhu, J.F. Lu, D.T. You, W. Xu, Z. Zhu, A.G. Manohari, F. Chen, Extra green light induced ZnO ultraviolet lasing enhancement assisted by Au surface plasmons, Nanoscale. 10 (2018) 623–627. doi:10.1039/C7NR07846C.

[54] T. Dixit, I.A. Palani, V. Singh, Insights into non-noble metal based nanophotonics: Exploration of Cr-coated ZnO nanorods for optoelectronic applications, RSC Adv. (2018). doi:10.1039/c7ra13174g.